PALEOCLIMATE

Tectonic degassing drove global temperature trends since 20 Ma

Timothy D. Herbert¹*†, Colleen A. Dalton¹†, Zhonghui Liu², Andrea Salazar³, Weimin Si¹, Douglas S. Wilson⁴

The Miocene Climatic Optimum (MCO) from ~17 to 14 million years ago (Ma) represents an enigmatic reversal in Cenozoic cooling. A synthesis of marine paleotemperature records shows that the MCO was a local maximum in global sea surface temperature superimposed on a period from at least 19 Ma to 10 Ma, during which global temperatures were on the order of 10°C warmer than at present. Our high-resolution global reconstruction of ocean crustal production, a proxy for tectonic degassing of carbon, suggests that crustal production rates were ~35% higher than modern rates until ~14 Ma, when production began to decline steeply along with global temperatures. The magnitude and timing of the inferred changes in tectonic degassing can account for the majority of long-term ice sheet and global temperature evolution since 20 Ma.

he climatic journey from global warmth to the great Pleistocene ice ages began many tens of millions of years ago, in the late Eocene (~40 Ma) when global temperatures began to descend from the strikingly warm conditions of the Mesozoic and Early Cenozoic (1). This path was far from monotonic, however. The climate system reached a tipping point at the Eocene/Oligocene boundary, when a substantial icecap grew on Antarctica and global temperatures declined. Episodic advances and retreats of this Southern Hemisphere icecap occurred for most of the Oligocene and Miocene (2, 3). However, an important reversal of the climatic trend occurred during the Miocene Climatic Optimum (MCO), when the East Antarctic Ice Sheet (EAIS) may have largely disappeared (4, 5).

The MCO was originally recognized by a substantial excursion to lighter values in the benthic oxygen isotope record, which could reflect a rise in deep sea temperatures or a decrease in global ice volume (1, 2, 6, 7). Although the partitioning of the two components remains challenging, it is clear that both warming and deglaciation occurred on and around the Antarctic continent (4, 5, 8). In Fig. 1, we provide a continuous global estimate of marine temperatures through the MCO by moving to higher latitudes where the pattern of temperature change is clear, although temperature changes are certainly amplified relative to a global mean ocean temperature. The curves rely almost entirely on the alkenone proxy, with a single exception in the Southern Hemisphere between an alkenone-based record at Deep Sea Drilling Project Site 594 (9) spliced to a continuous GDGT (glycerol dialkyl glycerol tetraether)-based estimate at Integrated Ocean Drilling Program Site 1352 over the MCO (10).

This synthesis of Miocene ocean temperatures indicates that the MCO was a local thermal maximum superimposed on a strikingly warm background climate. In comparison to the present day, temperatures preceding and postdating the MCO were high for millions of years: A global alkenone-based reconstruction at 10 Ma estimated an area-weighted ocean warming of +6°C relative to the present day (9); Fig. 1 suggests that temperatures prior to the MCO may have been similar. Estimating the global temperature anomaly during the MCO itself is difficult, because the temperatures were so warm that the alkenone proxy became saturated over a band of $\pm \sim 40^{\circ}$ latitude around the equator, implying temperatures in excess of ~29°C. However, by relying on regional Northern and Southern Hemisphere stacks where paleotemperatures remain below alkenone saturation, we arrive at an estimate of a global mean surface air temperature (SAT) anomaly of ~ +12° to 19°C using a scaling of ~1.7 times (11) the global sea surface temperature (SST) anomaly of +7.25° to 11.5°C (fig. S1). The warmth we estimate is on the high side of a recent estimate of MCO ΔSAT (+11.5°C) compiled from heterogeneous SST proxies, which includes tropical estimates of perhaps questionable reliability (12).

That the MCO represents a local maximum in global temperatures is also confirmed by high-resolution Mg/Ca records showing clear warming into the MCO that parallels the marine δ^{18} O curve at two tropical locations (13) and pronounced cooling at the end of the MCO at South Pacific ODP Site 1171 (14), supported by similar cooling in a GDGT-based record from the Arabian Sea (15). The link of inferred warming to deglaciation in Antarctica is

supported by micropaleontological and sedimentological observations of open water surrounding much of the Antarctic during the MCO (5), with vegetation occupying at least coastal areas of that continent during this time (8). A warm high-latitude Southern Ocean is also consistent with clumped isotope results on bottom-dwelling foraminifera that indicate MCO deep ocean temperatures ~10°C warmer than at present (16).

It is thus evident that Miocene warmth was global, long-lived, and peaked with the retreat of ice over much of Antarctica. Global cooling occurred with the reoccupation of much of the Antarctic by ice after the MCO, accelerating after ~ 9.5 Ma (Fig. 1).

Here, we investigated the possibility that global climate since 20 Ma was paced and synchronized by changes in a slow, but powerful, deep Earth process: the rate of degassing of CO_2 controlled by changes in the rate of oceanic plate creation and destruction. Our hypothesis builds on seminal work by Berner *et al.* (17), who proposed that on time scales longer than the residence time of carbon in the ocean-atmosphere-biosphere system (>100,000 years),

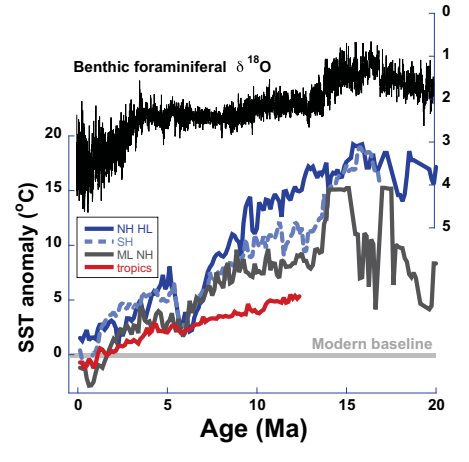


Fig. 1. Regionally averaged marine sea surface temperature anomalies relative to the present day, compared to the evolution of oxygen isotopic values of bottom-dwelling foraminifera. Data are from (7). Abbreviations: NH HL, Northern Hemisphere high latitude (45° to 69°N): SH. Southern Hemisphere (20° to 49°S); ML NH, midlatitudes of the Northern Hemisphere (29° to 43°N); Tropics, all tropical sites (24°N to 2°S). All paleotemperature determinations were made with the alkenone proxy, with the exception of Site 1352 (part of the Southern Hemisphere stack), where we rely on GDGT-based paleothermometry (data S1 and S2). Marine temperatures evolve essentially synchronously in both hemispheres and reach a local maximum at the time of the MCO. The large cooling from ~9.5 to 6 Ma is not reflected in the benthic record, presumably because there was little growth of continental ice during this period.

¹DEEPS, Brown University, Providence, RI 02912, USA. ²Department of Earth Sciences, University of Hong Kong, Hong Kong, China. ³Department of Earth and Planetary Science, Harvard University, Cambridge, MA, USA. ⁴Department of Earth Science, University of California, Santa Barbara, CA, USA.

^{*}Corresponding author. Email: timothy_herbert@brown.edu †These authors contributed equally to this work.

the inventory of CO2 in the atmosphere would be controlled by a plate tectonic degassing source term, buffered by the negative feedback of silicate weathering (18, 19). Most subsequent treatments of the long-term carbon cycle have instead focused on removal rates of carbon as the forcing function, often explicitly on the assumption that tectonic degassing has not changed appreciably (19-23). However, investigating the tectonic forcing of climate in the past 20 million years offers several key advantages over studies focused on longer time periods: The motions of tectonic plates are well known because of the preservation of young seafloor, magnetic polarity reversals are dated with high accuracy and small uncertainties. and large and well-dated transitions occurred in global climate.

We derived a global synthesis of ocean crust production rate, which we propose is a proxy for degassing rates over time (24). This assumption does not specify the proportion of degassing that occurs at mid-ocean ridges (25), in metamorphism in orogenic belts (26, 27), or by release in subduction zones (28-30), as faster crust production necessarily implies faster lithosphere destruction (and the converse). Our simple model neglects factors that are likely to be important in detail, such as the carbon content of sediments and rocks fed into orogenic and subduction zones, the dip of the subducting plate, and other factors that might influence the efficiency of tectonic degassing independently of the total rate of marine crustal recycling (28, 31).

Crustal production rates are calculated as the product of spreading rate and ridge length, assuming that crustal thickness is constant in space and time. Compilations of ocean crustal thickness have shown that it is largely independent of spreading rate except at ultraslow spreading ridges where melt supply is low (32). We took advantage of recent reconstructions of ocean ridge spreading histories at high temporal resolution (33–35) as well as new determinations of spreading rates in the eastern Pacific. Central to our analysis is a

careful treatment of three distinct sources of error: in the rotation parameters that describe seafloor spreading, in the endpoints of each mid-ocean ridge, and in the ages of magnetic polarity reversals.

The globally integrated crustal production curve reveals large changes since $\sim\!20$ Ma (24) (Fig. 2A). Total crustal production decreased from at least $3.3~{\rm km}^2/{\rm year}$ prior to 14 Ma to no more than $2.7~{\rm km}^2/{\rm year}$ after 6 Ma. Ridges in the eastern Pacific dominate total production (Fig. 2, B and C), but crust production has slowed along most ridges since 20 Ma. Only the Pacific-Antarctic ridge substantially increased production; ridges in the eastern Pacific reduced production by 25 to 50%, and those in the Atlantic slowed by 10 to 30%.

Previous studies of ocean crust production differ in their estimate of the trend since the mid-Miocene, ranging from increasing (36) to constant (37) to decreasing (38, 39). Among the subset of studies that identified declining ridge flux, our result has a larger amplitude, greater level of detail, and better-defined uncertainty. Three main factors may explain these improvements: an updated reconstruction of the complex and incomplete record of spreading in the eastern Pacific since 25 Ma, the inclusion of ridge spreading histories with higher temporal resolution, and our use of astronomically dated magnetic polarity ages (40, 41). Important pieces of the record of relative motion of the Cocos, Nazca, and Pacific plates are obscured by large microplates, poor low-latitude magnetic geometry, and hotspot tracks. Moreover, some studies (36, 37, 42) derive spreading rates from gridded estimates of seafloor age grid, early versions of which have been shown to contain some errors in the eastern Pacific for ages of 5 to 25 Ma (43). Although we compiled the eastern Pacific spreading record in more detail than previous authors, we caution that subdividing the interval from 22 to 15 Ma remains difficult because of the limited record of the Nazca-Pacific and Cocos-Nazca plate pairs. Other studies derive spreading rates from rotation

poles, as we do, but are focused on a longer time period and typically consider only two to four intervals within the past 20 Ma (36, 39), in contrast to our use of 10 intervals (table S3). Furthermore, relative to the CK95 time scale (44) used by many earlier studies, the astronomical polarity time scale used here (40) importantly shortens the interval from C5C to C6 (~16 to 19 Ma). The smaller errors in the astronomical dating of magnetic ages also reduce uncertainties in crust production rate and allow greater confidence to be assigned to the rate changes we measured (data S3).

The similarity of the new crust production rates to the broad evolution of ocean temperatures motivated us to evaluate the plausibility of two end-member explanations for cooling since the Miocene, one focused on changes in continental weatherability (CO_2 sink) and the other on CO_2 degassing (CO_2 source). The weatherability argument posits a long-term increase in the proportion of chemical weathering in relation to continental breakdown (19, 22) or to the emergence of maritime continents with easily weathered lithologies in the tropical Indo-Pacific in the Plio-Pleistocene (23).

To explore the alternative (source) scenario, we constructed a carbon cycle mass balance forced by the new crust production spreading curve, which is used as a proxy for tectonic carbon release (supplementary materials). Because nearly all plate pairs display a pattern similar to that of the global ensemble (Fig. 2A), we made the simplification that tectonic degassing scales linearly to the global ocean crustal production function. Two adjustable parameters can be optimized to satisfy the twin constraints of CO2 degassing rates and global temperatures: (i) the Earth system sensitivity that relates atmospheric CO₂ to long-term equilibrium global temperature (ESS), and (ii) the sensitivity of the silicate weathering negative feedback to temperature (Ea), which is believed to keep the carbon system in long-term balance. There is good reason to suspect that ESS is larger than a recent estimate (45) of 2.6° to 3.9°C per doubling of CO₂ [referred to as equilibrium climate

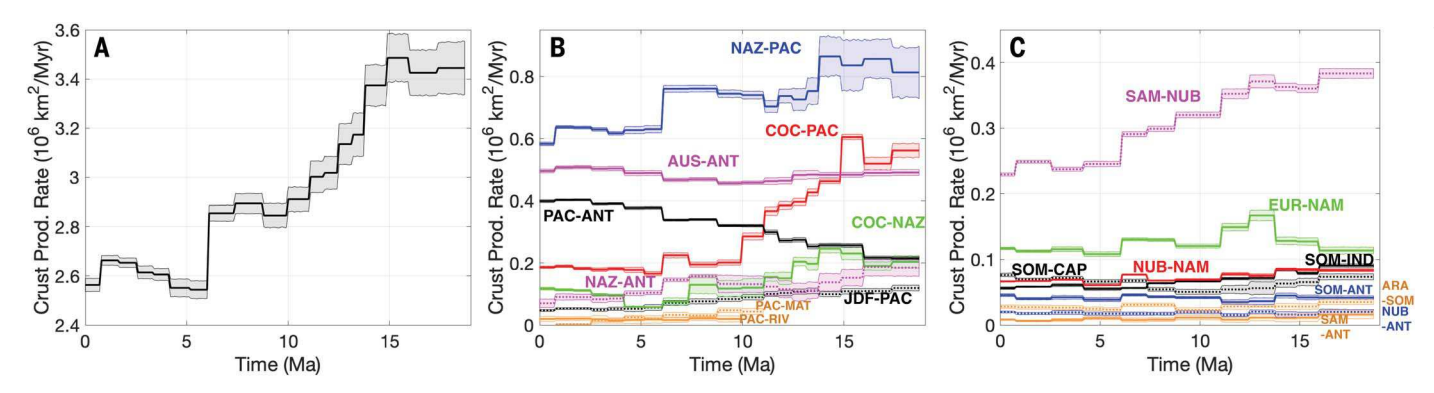
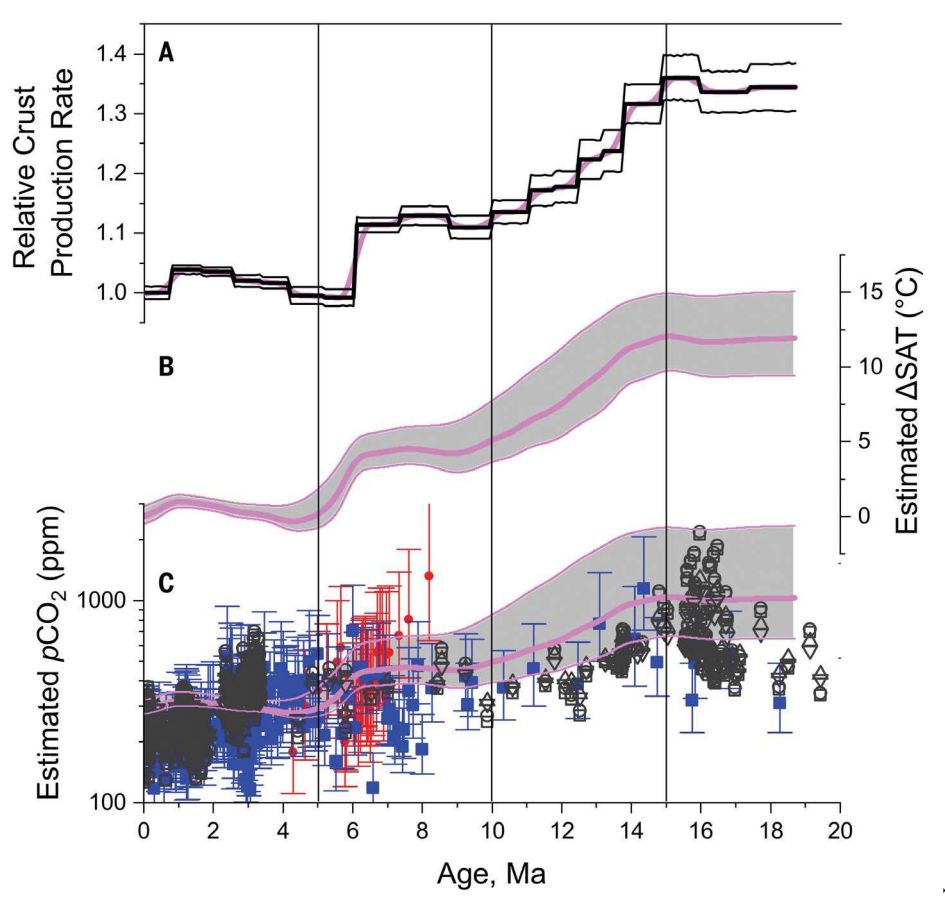


Fig. 2. Ocean crust production rates with 95% confidence interval. See data S3. (A) Global total. (B and C) By plate boundary. Note the different vertical scales for (B) and (C). See table S2 for plate names.

Fig. 3. Results of carbon mass balance modeling.

(A) Global degassing rate driven by ocean crustal production reconstruction. (B) Calculated changes in global surface air temperature (SAT). (C) Corresponding implied atmospheric CO₂ levels. Thick pink lines in (B) and (C) result from using central crustal production estimate [thick line in (A)]. Central carbon cycle parameters are Ea = 4 kcal/mol and ESS = 6.5°C per doubling of CO₂. Upper and lower bounds in (B) and (C) vary Ea from 3.5 to 4.5 kcal/mol and ESS from 5° to 8°C. Gray/ black symbols in (C) show pCO2 estimates from boron isotope analyses of planktonic foraminifera using different ocean carbon system parameters (49); blue and red symbols are based on carbon isotope values of alkenones (48, 50).



sensitivity (ECS or "Charney" climate sensitivity)] and also to consider the possibility that ESS may increase nonlinearly under high CO_2 (II, 46). We explored the effects of varying ESS between 5° and $8^\circ\mathrm{C}$ per CO_2 doubling, or approximately two times the 66th percentile bounds of the ECS (45). On tectonic time scales, ocean total dissolved inorganic carbon and alkalinity are primarily set by degassing, chemical weathering, and calcium concentration of seawater; therefore, it is not necessary to know the absolute values of these quantities a priori to estimate equilibrium $p\mathrm{CO}_2$ (supplementary materials).

The temperature dependence of weathering sensitivity is directly constrained by our estimate of peak MCO warmth and degassing. Here, *Ea* represents an effective weathering dependence on temperature in an Arrhenius formulation; it is a simple parameterization of the complex factors that control silicate weathering, including relief, the insulating effect of soil formation (transport limitation), and rainfall. The values chosen here, although considerably lower than those derived from pure silicate mineral activation energies, are consistent with previous studies of global weathering rates (supplementary materials).

The model satisfies the observation of generally warm early to mid-Miocene conditions, the timing of the MCO, and the steep cooling

observed globally in the younger half of the Miocene (14.5 to 6 Ma). The level of detail in the crustal production curve from ~14 to 20 Ma is limited by time resolution in tectonic constraints (rotation points at 13.739, 15.974, and 18.748 Ma) and by somewhat higher uncertainties in the astronomical calibration of the magnetic polarity time scale. Degassing rates may have changed very little since ~6 Ma (Fig. 2). If our proposed linkage between seafloor spreading and tectonic degassing is correct, it carries several major implications. First, the similarity in timing between crustal production changes and paleotemperatures suggests a geologically efficient (million-year time scale) coupling between tectonic processes and CO2 release to the Earth surface; time lags between tectonic forcing and climate response are not apparent at the resolution of our analysis. Second, it suggests that many proxy-based reconstructions of Miocene levels of CO₂ may be too low (Fig. 3C). The large range in plausible CO2 levels in our reconstruction derive from the wide permissible range of ESS. However, it is very difficult to reconcile the combination of peak Miocene warmth and high degassing with an atmospheric CO₂ inventory much lower than 850 ppm (12) (see Fig. 3). In this regard, we note that the trend of more recent CO₂ proxy estimates has been to revise reconstructed Miocene levels of CO₂ higher than earlier estimates (47-50),

although a gap remains between our preferred CO₂ curve (Fig. 3C, heavy pink line) and some proxy estimates. Last, our finding of large variations in seafloor spreading rate over the Neogene implies that interpretations of geochemical signals commonly used in paleoceanography (Mg/Ca, ⁸⁷Sr/⁸⁷Sr) may need to be reinterpreted in light of changing hydrothermal fluxes driven by changes in seafloor spreading rates (19, 51).

Forcing by a short-lived and relatively small input of CO2 from Columbia River basalt magmatism (52) appears insufficient as a firstorder explanation for the long duration of a strikingly warm Miocene climate, although it may have contributed to the apex during the MCO. In contrast, the hypothesis of long-term, large variations in tectonic degassing provides a potent, persistent driver. The evolution of temperature, inferred CO2 levels, and benthic δ^{18} O values (Figs. 1 and 3) suggests that polar glaciation exhibits strongly nonlinear threshold sensitivity to CO₂ and temperature: The large retreat of the East Antarctic Ice Sheet during the MCO may have required only a modest rise in CO2 from its generally high early Miocene level, and the onset of Northern Hemisphere ice ages at ~2.7 Ma occurred under tectonic CO₂ forcing similar to today. These results are consistent with two very different CO₂/temperature thresholds for glaciation in the Southern and Northern hemispheres proposed by (53) and especially imply a high sensitivity of East Antarctic ice volume to global temperature at a "set point" of $\sim +10^{\circ}$ C (Fig. 3).

We do not rule out the possibility that the global carbon cycle was also affected by a transition from weaker silicate "weatherability" in the Miocene relative to the Plio-Pleistocene (22, 23). However, the proposed low weatherability cannot serve as the primary explanation for the warm early to mid-Miocene: In the case of the scenario evaluated by Park et al. (23), a reduced MCO weatherability accounts for about one-fourth of the observed temperature anomaly (fig. S3). A 30% higher tectonic CO₂ flux rate will, however, generate enough warming to be consistent with our empirical SST and SAT estimates (Fig. 3). We readily admit that our temperature and CO2 model reconstructions are imperfect, because our assumptions that CO₂ degassing rate is in 1:1 proportion to ocean crustal production, and that weatherability and ESS remain fixed for the past 20 million years, are unlikely to apply strictly. In this regard, reduced weatherability during the mid-Miocene (22) may have enhanced large excursions in atmospheric CO₂ and temperature by reducing the sensitivity of the silicate weathering sink in a warm climate in comparison to the present day.

Our findings suggest that the coupled evolution of CO2 and climate over the Neogene can be understood as a combination of exogenous, slow forcing by the tectonic CO₂ source, in combination with more rapid but substantial repartitioning of the total surface carbon inventory among atmosphere, biosphere, and ocean paced by orbital cycles. Our study does not negate the rich possibility of other tectonic forcings of the carbon cycle (19-23, 29, 54), but it suggests that the dynamism in ocean crustal creation/destruction as a carbon cycle driver has been underestimated since the publication of (17). Riding on top of tectonic forcing, cyclical sequestration and release of carbon from the deep ocean (55) may explain highfrequency orbital-scale variability evident within the MCO, as demonstrated by cyclic variations in foraminiferal δ^{18} O-, δ^{13} C-, and Mg/ Ca-based SST estimates (4, 6, 13, 14, 56); processes driving the oceanic carbon reservoir became dominant during the Pleistocene ice ages.

REFERENCES AND NOTES

- J. Zachos, M. Pagani, L. Sloan, E. Thomas, K. Billups, Science 292, 686–693 (2001).
- B. P. Flower, J. P. Kennett, *Paleoceanography* 10, 1095–1112 (1995).
- D. Liebrand et al., Proc. Natl. Acad. Sci. U.S.A. 114, 3867–3872 (2017).
- R. Levy, D. Harwood, F. Florindo, SMS Science Team, Proc. Natl. Acad. Sci. U.S.A. 113, 3453-3458 (2016).
- F. Sangiorgi et al., Nat. Commun. 9, 317 (2018).
- A. Holbourn, W. Kuhnt, K. G. D. Kochhann, N. Andersen, K. J. Sebastian Meier, Geology 43, 123–126 (2015).
- D. De Vleeschouwer, M. Vahlenkamp, M. Crucifix, H. Pälike, Geology 45, 375–378 (2017).
- 8. S. Warny et al., Geology 37, 955-958 (2009).
- 9. T. D. Herbert et al., Nat. Geosci. 9, 843-847 (2016).
- 10. J. Jiang, thesis, University of Hong Kong (2019).
- 11. D. J. Lunt et al., Nat. Geosci. **3**, 60–64 (2009).
- N. J. Burls et al., Paleoceanogr. Paleoclimatol. 36, e2020PA004054 (2021).
- S. M. Sosdian, C. H. Lear, *Paleoceanogr. Paleoclimatol.* 35, e2020PA003920 (2020).
- A. E. Shevenell, J. P. Kennett, D. W. Lea, Science 305, 1766–1770 (2004).
- 15. G. Zhuang, M. Pagani, Y. G. Zhang, Geology 45, 655-658 (2017).
- S. E. Modestou, T. J. Leutert, A. Fernandez, C. H. Lear, A. N. Meckler, *Paleoceanogr. Paleoclimatol.* 35, e2020PA003927 (2020).
- R. A. Berner, A. C. Lasaga, R. M. Garrels, Am. J. Sci. 283, 641–683 (1983).
- J. C. Walker, P. Hays, J. F. Kasting, J. Geophys. Res. 86, 9776–9782 (1981).
- L. R. Kump, M. A. Arthur, in *Tectonic Uplift and Climate Change* (Springer, 1997), pp. 399–426.
- 20. M. Raymo, W. F. Ruddiman, Nature 359, 117-122 (1992).
- 21. G. Li, H. Elderfield, *Geochim. Cosmochim. Acta* **103**, 11–25 (2013).
- 22. J. K. Caves Rugenstein, D. E. Ibarra, F. von Blanckenburg, Nature 571, 99–102 (2019).
- Y. Park et al., Proc. Natl. Acad. Sci. U.S.A. 117, 25319–25326 (2020).
- C. A. Dalton, D. S. Wilson, T. D. Herbert, Geophys. Res. Lett. 49, e2022GL097937 (2022).
- A. E. Saal, E. H. Hauri, C. H. Langmuir, M. R. Perfit, *Nature* 419, 451–455 (2002).
- 431–433 (2002).
 J. A. Becker, M. J. Bickle, A. Galy, T. J. Holland, *Earth Planet*. Sci. Lett. 265, 616–629 (2008).
- 27. A. Skelton, Geology 39, 43-46 (2011).
- 28. C.-T. A. Lee et al., Geosphere **9**, 21–36 (2013).
- 29. N. R. McKenzie et al., Science 352, 444-447 (2016).
- P. B. Kelemen, C. E. Manning, Proc. Natl. Acad. Sci. U.S.A. 112, E3997–E4006 (2015).
- 31. T. Plank, C. E. Manning, Nature 574, 343-352 (2019).
- R. S. White, D. McKenzie, R. K. O'Nions, J. Geophys. Res. 97, 19683–19715 (1992).
- 33. S. Merkouriev, C. DeMets, *Geophys. J. Int.* **173**, 1064–1083 (2008).
- C. DeMets, S. Merkouriev, Geophys. J. Int. 207, 741–773 (2016).
- C. DeMets, S. Merkouriev, S. Jade, Geophys. J. Int. 220, 1149–1171 (2019).
- C. J. Rowan, D. B. Rowley, Geophys. J. Int. 208, 1173–1183 (2017).
- 37. D. B. Rowley, Geol. Soc. Am. Bull. 114, 927-933 (2002).
- 38. C. P. Conrad, C. Lithgow-Bertelloni, Geology 35, 29-32 (2007).
- 39. R. D. Müller et al., Tectonics 38, 1884-1907 (2019).
- F. J. Hilgen, L. J. Lourens, J. A. van Dam, in *The Geologic Time Scale 2012*, F. M. Gradstein, J. G. Ogg, M. Schmitz, G. Ogg, Eds. (Elsevier, 2012), pp. 923–978.

- 41. A. J. Drury et al., Earth Planet. Sci. Lett. 475, 254-266 (2017).
- 42. J.-P. Cogné, E. Humler, Geochem. Geophys. Geosyst. 7, Q03011 (2006).
- 43. D. B. Rowley, Lithosphere 11, 21-43 (2019).
- S. C. Cande, D. V. Kent, J. Geophys. Res. 97, 13917–13951 (1992).
- S. Sherwood et al., Rev. Geophys. 58, e2019RG000678 (2020).
- A. Farnsworth et al., Geophys. Res. Lett. 46, 9880–9889 (2019).
- S. M. Sosdian et al., Earth Planet. Sci. Lett. 498, 362–376 (2018).
- H. M. Stoll et al., Quat. Sci. Rev. 208, 1–20 (2019).
 J. W. B. Rae et al., Annu. Rev. Earth Planet. Sci. 49, 609–641 (2021).
- T. Tanner, I. Hernández-Almeida, A. J. Drury, J. Guitián,
 H. Stoll, *Paleoceanogr. Paleoclimatol.* 35, e2020PA003925 (2020)
- J. A. Higgins, D. P. Schrag, Earth Planet. Sci. Lett. 416, 73–81 (2015).
- 52. J. Kasbohm, B. Schoene, Sci. Adv. 4, eaat8223 (2018).
- 53. R. M. Deconto et al., Nature 455, 652-656 (2008).
- S. Brune, S. E. Williams, R. D. Müller, *Nat. Geosci.* 10, 941–946 (2017).
- D. Archer, A. Winguth, D. Lea, N. Mahowald, Rev. Geophys. 38, 159–189 (2000).
- A. Holbourn, W. Kuhnt, M. Schulz, J.-A. Flores, N. Andersen, Earth Planet. Sci. Lett. 261, 534–550 (2007).

ACKNOWLEDGMENTS

We thank A. Lee, C. Carchedi, and J. Smith for assistance with seafloor magnetic anomaly studies. This research used samples and/or data provided by the International Ocean Discovery Program (IODP) and its predecessors. IODP is sponsored by NSF and participating countries under management of Joint Oceanographic Institutions (JOI) Inc. Funding: Supported by NSF grants 1635127 (T.D.H., W.S., C.A.D.) and 1545859 (T.D.H.), the Doherty Fund for Oceanography at Brown University (T.D.H., W.S.), Hong Kong Research Grants Council grant 17305019 (Z.L.), and the Leadership Alliance (A.S.). Author contributions: Conceptualization, T.D.H., C.A.D.; methodology, T.D.H., C.A.D., Z.L., A.S., W.S., D.W.; writing-original draft, T.D.H., C.A.D., Z.L., A.S., W.S., D.S.W.; writing-reviewing and editing, T.D.H., C.A.D., W.S., D.S.W. Competing interests: The authors declare no competing interests. Data and materials availability: The data supporting the regional SST trends in Fig. 1 include previously published (9, 57-66) data available at the PANGAEA data repository (www.pangaea.de). Data tables providing new TEX₈₆ based estimates of SST and bulk stable isotopes at Site U1352, the age model used for Site U1352, and the regional SST stacks presented in Fig. 1 are also archived at the PANGAEA data repository. License information: Copyright © 2022 the authors, some rights reserved; exclusive licensee American Association for the Advancement of Science. No claim to original US government works, www.science.org/about/science-licensesiournal-article-reuse

SUPPLEMENTARY MATERIALS

science.org/doi/10.1126/science.abl4353 Supplementary Text Figs. S1 and S2 Tables S1 and S2 Data S1 to S4 Matlab Codes for Carbon Cycle Calculations References (57–86)

Submitted 16 July 2021; accepted 3 May 2022 10.1126/science.abl4353



Tectonic degassing drove global temperature trends since 20 Ma

Timothy D. HerbertColleen A. DaltonZhonghui LiuAndrea SalazarWeimin SiDouglas S. Wilson

Science, 377 (6601), • DOI: 10.1126/science.abl4353

Crustal effects on climate

Why was the long-term global cooling trend of the Cenozoic interrupted by a several-million-year interval of warming during the middle of the Miocene? Herbert *et al.* present a reconstruction of global ocean crustal production to show that tectonic degassing of carbon can account for most of the long-term ice sheet and global temperature evolution for the past 20 million years (see the Perspective by von der Heydt). These results provide further support for the idea that sea floor spreading rates can control global changes in climate. —HJS

View the article online

https://www.science.org/doi/10.1126/science.abl4353

Permissions

https://www.science.org/help/reprints-and-permissions

Use of this article is subject to the Terms of service